Journal of Computational Physics 229 (2010) 1381–1400

Contents lists available at ScienceDirect

Journal of Computational Physics

journal homepage: www.elsevier.com/locate/jcp

Atomistic hybrid DSMC/NEMD method for nonequilibrium multiscale simulations

Kai Gu [a], Charles B. Watkins [a,*], Joel Koplik [b]

[a] Department of Mechanical Engineering, The City College of CUNY, 160 Convent Ave., New York, NY 10031, USA
[b] Benjamin Levich Institute and Department of Physics, The City College of CUNY, 160 Convent Ave., New York, NY 10031, USA

ARTICLE INFO

Article history:
Received 11 December 2008
Received in revised form 26 July 2009
Accepted 19 October 2009
Available online 28 October 2009

Keywords:
Direct simulation Monte Carlo
Nonequilibrium molecular dynamics
Hybrid simulations
Coupled method, multiscale simulation
Molecular collision model
Solid–gas interface
Particle simulation methods

ABSTRACT

A multiscale hybrid method for coupling the direct simulation Monte Carlo (DSMC) method to the nonequilibrium molecular dynamics (NEMD) method is introduced. The method addresses Knudsen layer type gas flows within a few mean free paths of an interface or about an object with dimensions of the order of a few mean free paths. It employs the NEMD method to resolve nanoscale phenomena closest to the interface along with coupled DSMC simulation of the remainder of the Knudsen layer. The hybrid DSMC/NEMD method is a particle based algorithm without a buffer zone. It incorporates a new, modified generalized soft sphere (MGSS) molecular collision model to improve the poor computational efficiency of the traditional generalized soft sphere GSS model and to achieve DSMC compatibility with Lennard-Jones NEMD molecular interactions. An equilibrium gas, a Fourier thermal flow, and an oscillatory Couette flow, are simulated to validate the method. The method shows good agreement with Maxwell–Boltzmann theory for the equilibrium system, Chapman–Enskog theory for Fourier flow, and pure DSMC simulations for oscillatory Couette flow. Speedup in CPU time of the hybrid solver is benchmarked against a pure NEMD solver baseline for different system sizes and solver domain partitions. Finally, the hybrid method is applied to investigate interaction of argon gas with solid surface molecules in a parametric study of the influence of wetting effects and solid molecular mass on energy transfer and thermal accommodation coefficients. It is determined that wetting effect strength and solid molecular mass have a significant impact on the energy transfer between gas and solid phases and thermal accommodation coefficient.

1. Introduction

With continued improvements in computer speed and storage capabilities, atomistic simulation methods, such as direct simulation Monte Carlo method (DSMC) and molecular dynamics (MD), have become increasingly viable options for gas dynamics research at sub-macroscopic scales. The scales of interest are distinguished by a flow Knudsen number ($Kn = \lambda/d$), the ratio of mean free path to a characteristic flow dimension, greater than 0.1.

DSMC, in particular, has been widely applied to investigate dilute gas flow phenomena at length scales on the order of a mean free path that are no longer governed by continuum fluid dynamics but are in the transition regime between continuum and free molecular flow ($0.1 \leqslant Kn \leqslant 10$). Knudsen layer type gas flows within a few mean free paths of an interface or about an object with dimensions of the order of a few mean free paths are in the transition regime.

* Corresponding author. Tel.: +1 212 650 5439; fax: +1 212 650 8013.
E-mail address: watkins@ccny.cuny.edu (C.B. Watkins).

0021-9991/$ - see front matter © 2009 Elsevier Inc. All rights reserved.
doi:10.1016/j.jcp.2009.10.035

When applied to flow over an interface, the relatively efficient DSMC method has significant limitations in its ability to address the important nanoscale interactions of gas molecules with solid or liquid molecules comprising the interface. The present research is aimed at removing this limitation with the development of a hybrid, multiscale simulation method that uses the MD method to resolve nanoscale phenomena closest to the interface along with DSMC simulation of the remainder of the Knudsen layer. Thus, the method spans the disparate scales of molecular diameters and molecular collisions. (For argon at standard conditions, the mean free path is 63 nm, while the effective hard sphere molecular diameter is 0.4 nm.) The nanoscale domain resolved near the interface may be a small but not insignificant portion of the Knudsen layer. We adopt the convention of referring to the overlapping scales of these flow domains and their resident phenomena as mesoscale.

The DSMC method was originally developed by Bird [1] and subsequent developments have been catalogued by Orhan et al. [2], and Prasanth and Kakkassery [3]. It has produced strikingly accurate results in a variety of dilute gas flow simulations by introducing the notion of stochastic representative particles in place of actual gas molecules. The simulation divides tracks the motions and collisions of these particles through a flow domain, which is divided into cells, by simplified molecular interaction mechanics. DSMC collisions take place with kinetic outcomes determined by modeled molecular scattering probabilities. Macroscopic flow properties are computed from sampled particle statistics over a number of independent simulation trials, represented by ensemble or time averages. A binary collision assumption limits DSMC simulation to dilute gases.

DSMC requires interface boundary conditions for the simulation particles. These are necessarily restricted to simplified mechanical models based on average surface collision dynamics or to statistically averaged particle flux distributions based on simplified molecular interactions at the interface. Since DSMC simulation is limited to dilute gases with simplified boundary interactions, it cannot resolve complex mesoscale interfacial phenomena involving interphase molecular interaction and exchange at an interface.

Classical molecular dynamics simulation or MD dates from its conception by Alder and Wainwright [4] in the late 1950s. Its history and algorithms are described in a number of texts and reference works (e.g., [5, 6]). It is essentially a simulation method that tracks the motions of modeled individual atoms, molecules, molecular clusters, or ions. MD is based on applying Newtonian mechanics to these motions with interparticle attractive and repulsive forces determined by specified potential energy functions. Most commonly, short range interactive forces are derived from a Lennard-Jones (L-J) intermolecular potential function.

The MD method is appealing for interfacial physics because it can model interaction of individual gas molecules with the liquid or solid molecules comprising a multiphase interface and can also model interphase transitions. Furthermore, it is not restricted to dilute gases and can simulate the motions of denser gases and liquid near the interface. Technically, when the MD method is applied to fluids that are not in equilibrium because they are subjected to imposed mechanical or thermal drivers, it is known as nonequilibruim molecular dynamics (NEMD).

The substantial disadvantage of MD or NEMD simulation is that it is so highly computationally intensive that its application is restricted to nanoscale systems comprised of relatively small numbers of molecules within dimensions of hundreds of nanometers. It cannot be applied to analyze mesoscale flow systems of engineering interest since it is infeasible to simultaneously apply it to the interfacial region and the larger, bulk incident-gas region. Nevertheless, it is a valuable tool for investigating interfacial physics. As in the case of DSMC, macroscopic properties can be obtained by sampling.

A multiscale method with the ability to efficiently simulate the molecular gas dynamics of bulk microscale flow over an interface, while resolving the computationally demanding nanoscale molecular interactions in a domain surrounding the interface, would be invaluable. The ability of DSMC and NEMD to handle molecular collision-scale and molecular diameter-scale types of problems, respectively, suggests that a hybrid, combing the two, could be an effective approach to development of a robust multiscale method.

Hybrid simulation schemes are abundant for microscale/continuum gas flows using DSMC coupled with Navier–Stokes, Stokes, or Euler continuum CFD methods [7–10]. Likewise, many approaches have been developed for NEMD coupled with continuum Navier–Stokes CFD for nanoscale/microscale liquid flows [11–16]. However, there has been far less work on hybridized DSMC/NEMD methods and the methods that have been developed, so far, either have substantial limitations or are untested for their ability to model certain important systems.

A combined DSMC and NEMD study of laser ablation was reported by Zeifman et al. [17] in which information was transferred from a NEMD flow domain to a DSMC flow domain but there was no two-way active coupling between the two domains. A hybrid DSMC/NEMD gas/solid simulation method for one-way DSMC to near-surface NEMD matching, which involves repositioning of incident DSMC molecules, was developed by Yamamoto et al. [18].

A simulation method was developed by Nedea et al. [19,20], coupling NEMD solution domains to Monte Carlo (MC) solution domains. The MC method used is an extension of DSMC [1] that avoids the restriction of traditional DSMC to dilute gases. The primary emphasis of their work is on dense hard-sphere gas systems but they also demonstrate good results for thermally driven flow in a dilute gas channel bounded by isothermal walls [20]. However, their hybrid method is coupled by matching the macroscopic properties in overlapping buffer layers, and not focused on ensuring mass, momentum, and heat flux continuity across the method interface. This and the modeling artifices they employed may make it difficult for their method to completely capture the physics of systems with large gradients in the method interface region or unsteady flows.

In this article we introduce a new DSMC/NEMD hybrid method based on DSMC particle/NEMD molecule coupling with consistent particle flux dynamics across the interface between separate DSMC and NEMD solution domains. In developing

our hybrid method, special attention was paid to the molecular collision model in the DSMC domain to insure compatibility near the interface with the Lennard-Jones (L-J) intermolecular potential function used in the NEMD domain. A new collision model with improved efficiency and low-temperature capability that is suitable for maintaining compatibility was also developed and implemented.

We present the results of validating the particle flux continuity at the DSMC/NEMD interfaces in both equilibrium and nonequilibrium systems by comparisons with Maxwellian and Chapman Enskog theory, respectively. To verify the method's accuracy in unsteady systems, an oscillatory Couette flow simulation was compared with a pure DSMC solution. In addition, the hybrid method's computational efficiency was compared with that of the pure NEMD method for different DSMC/NEMD solver partition size ratios and system particle numbers.

Finally, the hybrid method was applied to investigate interaction of argon gas with solid surface molecules in a mesoscale parametric study of the influence of wetting effects and solid molecular mass on energy transfer and thermal accommodation coefficients. The results are compared with results from DSMC simulations using the thermal accommodation coefficients determined from the hybrid simulations.

2. DSMC molecular collision modeling

Various molecular collision cross section models have been developed for use in DSMC through consideration of the intermolecular force or potential. For DSMC applications, the goal generally is to reproduce the dependence of viscosity and self diffusion on temperature of actual gases. The traditional and most widely used collision model is the variable hard sphere (VHS) model [1]. Some newer molecular collision models, such as the variable soft sphere (VSS) [21] and the generalized hard sphere (GHS) [22], have been developed to replicate more closely the actual viscosity cross section behavior of gas molecules for certain interaction potentials. The modified general hard sphere (MGHS) [23] model was developed to improve on the computational efficiency of the GHS model, which in its original form was an excessive DSMC computational burden. The MGHS model also improved low temperature performance over the GHS model.

Fan [24] proposed a physically more accurate model, generalized soft sphere (GSS), by deriving a Lennard-Jones potential function-based collision cross section, dependent on particle collision speed. The L-J (12-6) potential function,

$$V(r_{ij}) = 4\varepsilon\left[\left(\frac{\sigma}{r_{ij}}\right)^{12} - \varepsilon_{sg}\left(\frac{\sigma}{r_{ij}}\right)^{6}\right] \tag{1}$$

is commonly used to determine the intermolecular forces in molecular dynamics simulations and was adopted for the NEMD domain of our hybrid simulations. It characterizes both the short range repulsive forces as well as the longer range weakly attractive forces. In Eq. (1) , r_{ij} is the distance between molecule i and molecule j; ε and σ are the characteristic energy and interaction lengths, respectively. ε_{sg} is a parameter that is not present for interactions between gas molecules but is introduced for gas–surface molecule interactions and describes the wetting effect at the gas–solid interface. It would be assigned a value of 1.0 for complete wetting. A value of 0.75 would be partial wetting and values less than 0.5 are considered nonwetting.

Since the GSS model replicates most closely the intermolecular physics in the NEMD implementation of Eq. (1), it is more compatible with interfaces between NEMD and DSMC domains than the other collision models. Therefore, it would seem to be a good choice for the DSMC collision model in our hybrid method. However, if implemented as developed by Fan [24], GSS, like GHS, is computationally inefficient because its parameters cannot be obtained explicitly. A new, modified GSS (MGSS) model is introduced here, patterned after the MGHS model developed from GHS. We will show that MGSS improves computational efficiency and low temperature accuracy over GSS.

In the no-time counter (NTC) DSMC procedure [1], the number of candidate collision pairs from each cell is determined as

$$N_c = \frac{N\overline{N}F_N(\sigma_T c_r)_{\max}\Delta t}{2V_c} \tag{2}$$

where N is the number of molecules in the cell, $\overline{N}$ is the average number of molecules in the cell, F_N is the number of real molecules represented by the simulated one. $(\sigma_T c_r)_{\max}$ is the maximum value of the product of total cross section and relative velocities; i.e., the maximum pairwise collision probability; and V_c is the collision sampling cell volume. Subcells are used to increase the likelihood of collision pairs taking place between near neighbors. Collisions are accepted if

$$R_f < \frac{\sigma_T c_r}{(\sigma_T c_r)_{\max}} \tag{3}$$

where R_f is a uniformly distributed random number. To implement the GSS model, the total cross section can be written as follows:

$$\frac{\sigma_T}{\sigma^2} = \sum_j \beta_j \left(\frac{E_t}{\varepsilon}\right)^{l_j} \tag{4}$$

where $E_t = \frac{1}{2} m_r c_r^2, m_r$ is the reduced mass of two colliding molecules, and β_j and l_j are constants that are determined from a numerical least-squares fit of the coefficients of viscosity

$$\mu = \frac{5}{16}\left(\frac{\sqrt{\pi m k_B T}}{\pi \sigma^2 \Omega^{(2,2)^*}}\right) \tag{5}$$

and self-diffusion

$$D = \frac{3kT}{16p}\left(\frac{\sqrt{2\pi k_B T/m_r}}{\pi \sigma^2 \Omega^{(1,1)^*}}\right) \tag{6}$$

for a simple gas in which m is the particle mass, T is the temperature, p is pressure and k_B is the Boltzmann constant, and $\Omega^{(1,1)^*}$ and $\Omega^{(2,2)^*}$ represent integral relations [24,25] for computing the two transport coefficients from the L-J potential. Fan's GSS model [24] uses a two term formula for the diffusion and viscosity integrals, $\Omega^{(1,1)^*}$ and $\Omega^{(2,2)^*}$, to fit the data tabulated by Hirschfelder et al. [25] from numerical evaluation of the integrals. Fan's fitting results are shown in Figs. 1 and 2.

The GSS model [24] has significant limitations on its implementation in a DSMC simulation. One issue is that its total cross section tends toward infinity when particles encounter low relative speed collisions. Based on Eqs. (2) and (3), this means that the number of collision candidates tested inevitably increases while the probability of a successful selection decreases during the DSMC collision algorithm. Hence, the computational expense increases due to both increased collision candidates and the testing necessary to determine collision pairs.

For the GSS model the mean pairwise collision probability can be written from Eq. (4) as

$$\overline{c_r \sigma_T} = \sigma^2 \int\int \sum \beta_j \left(\frac{\frac{1}{2} m_r}{\varepsilon}\right)^{l_j} c_r^{2l_j+1} f_1 f_2 d\mathbf{c}_1 d\mathbf{c}_2 \tag{7}$$

in which f_1 and f_2 are the distribution functions of the collision pair, which has masses, m_1 and m_2. This probability, then, is a function of temperature with the resulting mean collision frequency, $\nu = n\overline{c_r \sigma_T}$, where n is the number density.

The dependence of pairwise collision probability on relative collision velocity is shown in the normalized plot of Fig. 3. The figure shows that the GSS collision probability rises in an unphysical manner with decreasing relative speed, eventually tending to infinity. In addition to lower computational efficiency, this results in unphysical, large collision frequencies for GSS due to the larger mean values determined from Eq. (7). These effects are particularly significant to simulation efficiency and accuracy at lower temperatures, where molecules are actually physically more inert.

To eliminate the unphysical characteristics of GSS, instead of defining the cross section uniformly as polynomials, our MGSS model follows an approach similar to that used by Macrossan and Lilley [23] for development of the MGHS model. In particular, we modified the GSS model with a cut-off speed for the higher-order polynomial function such that it is linear below it. The result is

$$(c_r \sigma_T)_{\mathrm{MGSS}} = \begin{cases} k(a) c_r + b(a) & c_r < a \\ \sigma^2 \sum \beta_j \left(\frac{\frac{1}{2} m_r}{\varepsilon}\right)^{l_j} c_r^{2l_j+1} & c_r > a \end{cases} \tag{8}$$

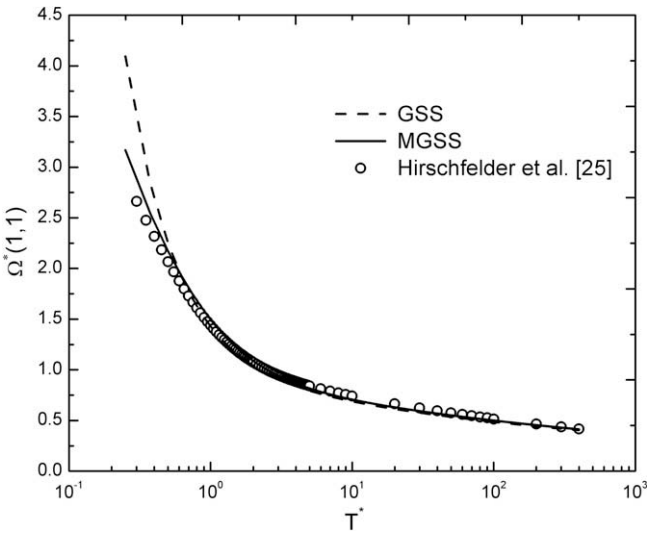

Fig. 1. Comparison of viscosity integral versus normalized temperature for collision models. The temperature is normalized by $\frac{\varepsilon}{k_B}$; for argon $\frac{\varepsilon}{k_B} = 120$ K.

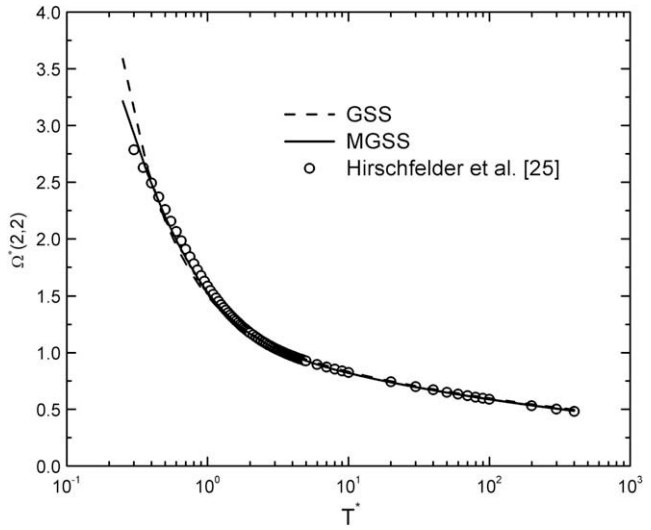

Fig. 2. Comparison of diffusion integral versus normalized temperature for collision models. The temperature is normalized by $\frac{\varepsilon}{k_B}$; for argon $\frac{\varepsilon}{k_B} = 120$ K.

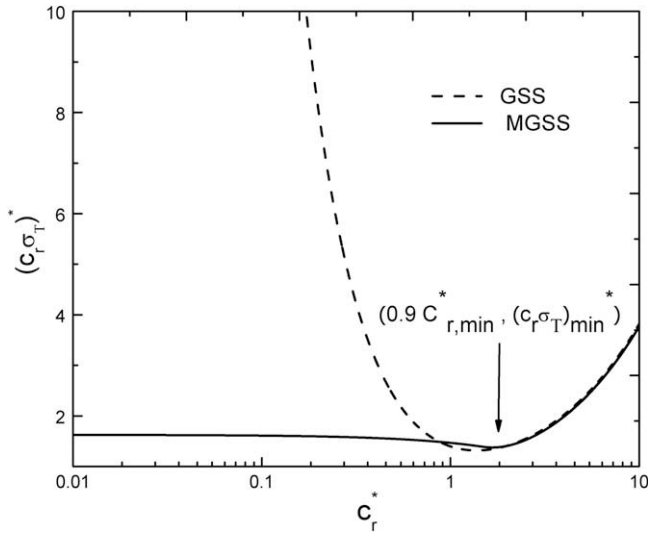

Fig. 3. Comparison of modeled normalized collision probability, $(C_r\sigma_T)^*$, versus normalized relative speed, C_r^*. Relative speed is normalized by the most probable velocity, $\sqrt{\frac{2k_BT_{ref}}{m}}$ and $C_r\sigma_T$ is normalized by $\overline{C_r\sigma_T}$, Eq. (11), at reference temperature, $T_{ref} = 273$ K.

where to maintain first-derivative continuity, k is the slope of the $c_r\sigma_T$ curve (as shown in Fig. 3) at the cut-off speed, a, and b is chosen to make the curve continuous at the cut-off speed, a. Therefore,

$$k(a) = \sigma^2 \sum \beta_j (2l_j + 1) \left(\frac{\frac{1}{2} m_r a^2}{\varepsilon} \right)^{l_j} \tag{9}$$

and

$$b(a) = \sigma^2 \sum \beta_j \left(\frac{\frac{1}{2} m_r}{\varepsilon} \right)^{l_j} a^{2l_j+1} - ak(a) \tag{10}$$

By reducing the order of total cross section at low relative speed, and limiting the polynomial at higher speed to order two, $\overline{c_r\sigma_T}_{\mathrm{MGSS}}$ can be obtained in the form:

$$(\overline{c_r\sigma_T})_{\mathrm{MGSS}} = AI_1(I_{21} + I_{22}) \tag{11}$$

where

$$A = \frac{2(m_1 m_2)^{3/2}}{\pi (k_B T)^3} \tag{12}$$

$$I_1 = \frac{\sqrt{\pi}(2k_B T)^{3/2}}{4(m_1 + m_2)^{3/2}} \tag{13}$$

$$I_{21} = \frac{1}{2}\left(k(a)\left(\frac{2k_B T}{m_r}\right)^2 \gamma\left(2, \frac{a^2 m_r}{2k_B T}\right) + b\left(\frac{2k_B T}{m_r}\right)^{\frac{3}{2}} \gamma\left(\frac{3}{2}, \frac{a^2 m_r}{2k_B T}\right)\right) \tag{14}$$

$$I_{22} = \frac{1}{2}\sigma^2 \sum_j \beta_j \left(\frac{m_r}{2\varepsilon}\right)^{l_j} \left(\frac{2k_B T}{m_r}\right)^{l_j+2} \Gamma\left(l_j + 2, \frac{a^2 m_r}{2k_B T}\right) \tag{15}$$

and $\Gamma(s,x)$ and $\gamma(s,x)$ are the upper and lower incomplete gamma functions, defined as

$$\Gamma(s,x) = \int_x^\infty t^{s-1} \exp(-t) dt \tag{16a}$$

$$\gamma(s,x) = \int_0^x t^{s-1} \exp(-t) dt \tag{16b}$$

Based on numerical experimentation, we selected a set of parameters that matches the Hirschfelder et al. [25] data quite well, $\beta_1 = 4.0, \beta_2 = 7.0, l_1 = -0.137$ an $l_2 = -1.55$ with $\alpha = 1.4$ for argon, and $a = 0.9 c_{r,\min}$, in which $c_{r,\min}$ is the value at the minimum of the GSS $c_r \sigma_T$ curve, as illustrated in Fig. 3.

The improvement in low relative speed behavior of the MGSS model over the GSS model is obvious in Fig. 3. Fig. 4 shows that the MGSS model also improves the mean collision frequency behavior at low temperature over the GSS model. Hence, both the computational efficiency and low temperature behavior are significantly improved.

Referring back to Figs. 1 and 2, the comparisons of $\Omega^{(1,1)^*}$ and $\Omega^{(2,2)^*}$ for GSS and MGSS clearly demonstrate that our new MGSS model achieves substantial improvements in the viscosity and diffusion coefficients at low temperature, compared with the GSS model. However, in typical applications of DSMC, the primary advantage of MGSS over GSS is its computational efficiency. The pure DSMC and hybrid DSMC/NEMD simulations presented herein, unless otherwise noted, all employed MGSS collision modeling.

3. Description of DSMC/MD hybrid method

In most hybrid methods that divide the physical domain to two or more parts and assign each one to different method solver, matching is achieved by establishing overlapping or "buffer" regions along the interfaces between the methods extending into their respective domains, wherein both methods are applied. The mean properties and momentum or heat fluxes from each domain are "copied" to the buffer, to generate the mean properties or flux continuities between the methods.

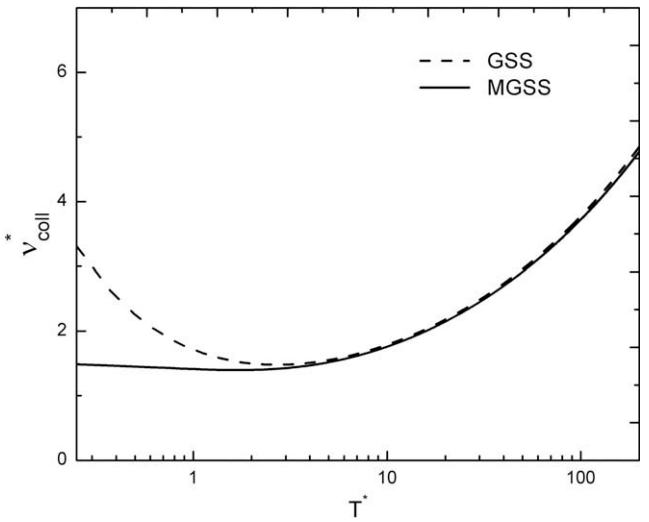

Fig. 4. Normalized mean collision frequency versus normalized temperature. The temperature is normalized by $\frac{\varepsilon}{k_B}$; for argon $\frac{\varepsilon}{k_B} = 120$ K; the collision frequency is normalized by the $4\rho k_B T_{ref}/\pi\mu_{ref}^{MGSS}$, where k_B is the Boltzmann constant; T_{ref} and μ_{ref}^{GSS}, Eq. (5), are taken at 273 K.

Wang and He [11] recently reviewed the various continuum/NEMD hybrid methods and proposed a new flux-based method for unsteady continuum/NEMD problems based on the introduction of an external force acting on the NEMD molecules. Likewise, Delgado-Buscalioni and Coveney [14] developed an unsteady flux-based hybrid method for continuum/NEMD coupling, introducing a fictitious force acting on the NEMD molecules to compensate for the momentum flux discontinuity across the continuum/NEMD interface. In principle, sampled DSMC domain results could be used as the basis for adapting a continuum/NEMD hybrid method for use as a DSMC/NEMD hybrid. However, issues such as the effect of force additions in creating non-physical density gradients and the need to maintain molecular energy and momentum conservation in individual molecular interactions discourage it. Furthermore, information is lost in the process of sampling and reconversion to a particle focus.

The basic hybrid steps we employed were quite simple. First, a one-to-one correspondence of DSMC particles to molecules was established, as opposed to the usual DSMC implementation of representing actual molecules with a far fewer number of simulation particles. Hence, the present simulation in the DSMC domain is computationally expensive compared with the usual DSMC simulation but, as we will show, the overall computational burden of our hybrid method is largely determined by the NEMD portion of the simulation.

The NEMD molecules in the present examples were initially deployed in a FCC arrangement. Then, the simulation was begun and they were allowed to migrate until an equilibrium state was reached. At that point, the barrier between the DSMC and NEMD domains was removed, allowing all particles to travel through each domain freely by the algorithm we developed.

For computational efficiency, the DSMC time steps are larger than the NEMD time steps (one DSMC time step is equal to several NEMD steps). Therefore, the coupling procedure synchronizes the DSMC computation with the NEMD computation at the beginning of each DSMC time step. The DSMC and NEMD computations then proceed in parallel.

In the DSMC domain, the DSMC method dictates that particles move freely throughout the DSMC time step with their trajectories determined by their velocity vectors at the beginning of the time step. Particle collisions take place instantaneously at the end of the time step. The collision algorithm determines the particle velocity vectors for the next time step. In the coupling procedure, we identify those DSMC particles with velocity vectors that will carry them across the boundary into the NEMD domain during the DSMC time step. We then remove these particles from the DSMC domain and copy them into their corresponding locations in a fictitious free-flight particle region adjacent to the NEMD boundary. These free-flight particles enter the NEMD domain to become NEMD molecules during the NEMD time stepping process according to their DSMC determined trajectories.

The purpose of creating a fictitious free flight region adjacent to the NEMD domain is to facilitate assigning the DSMC and NEMD domains to separate processors with communication required only during the synchronization process. It is, in effect, a "ghost" DSMC particle region that facilitates particle exchange during synchronization. NEMD molecules inside the NEMD domain do not interact with the particles in the free flight region until they enter the NEMD domain. When these particles do enter the NEMD domain, they encounter an insertion procedure that avoids an overlap in positions with the NEMD molecules already inside.

Some NEMD particle insertion algorithms (e.g., [26]) have been developed to minimize the influence on system potential energy of particle insertion too close to another particle. But for the dilute gas, particle spacing is usually larger than the interaction cut-off distance, r_c. Hence, we can avoid a complex insertion routine by directly creating a new NEMD particle in the position, where the free-flight particle enters the NEMD region with its DSMC velocity. If the distance between the new NEMD particle created and the existing NEMD particles is exceptionally small or actually overlaps with an existing NEMD particle, this new particle is randomly shifted in the neutral direction (i.e., z direction) to fulfill the criteria for the smallest distance allowed. In this work, we choose a minimum distance equal to σ, based on the observation that the peak of the radial distribution function (RDF) is around σ for a dilute gas.

NEMD molecules also escape from the NEMD region to become free-flight particles in the fictitious free-flight region. These out flux NEMD particles are removed in the NEMD solver, but keep moving in the free-flight region with their NEMD velocity vectors as NEMD time is advanced. When the NEMD time steps are synchronized with the DSMC step, new DSMC particles are created from these former NEMD particles and inserted into the DSMC domain with their position in the DSMC domain corresponding to their free-flight region position at synchronization.

The details are illustrated in Fig. 5. The present hybrid method ensures particle conservation and does not lose molecular information (i.e., velocities and positions) in its coupling steps, hence, mean flow property and flux values match implicitly. It should be easily extendable to couple across an interface between three-dimensional flow domains because in the free flight zone, particles are moving in three dimensions. No directional vector information is lost in the zone so the three-dimensional momentum components, as well as energy, are conserved.

In general, the free flight zone is a fictitious dilute gas region of arbitrary shape overlaying a portion of the DSMC domain that is adjacent to the NEMD domain. In applications where this method is likely to be useful, the physical region occupied by dilute gas is at least mesoscopic in size, and a subregion away from boundaries delimited by smooth surfaces can always be identified. This includes geometrically three-dimensional flow regions, which can be handled unambiguously with our method.

One parameter that must be set for the DSMC/NEMD hybrid is the time step. DSMC has a larger particle interaction time scale than NEMD. To avoid a low particle exchange frequency at the interface and possible momentum loss, we set $\Delta\tau_{\mathrm{DSMC}} = 20\Delta\tau_{\mathrm{MD}}$, which is equal to the NEMD Verlet list update interval [4].

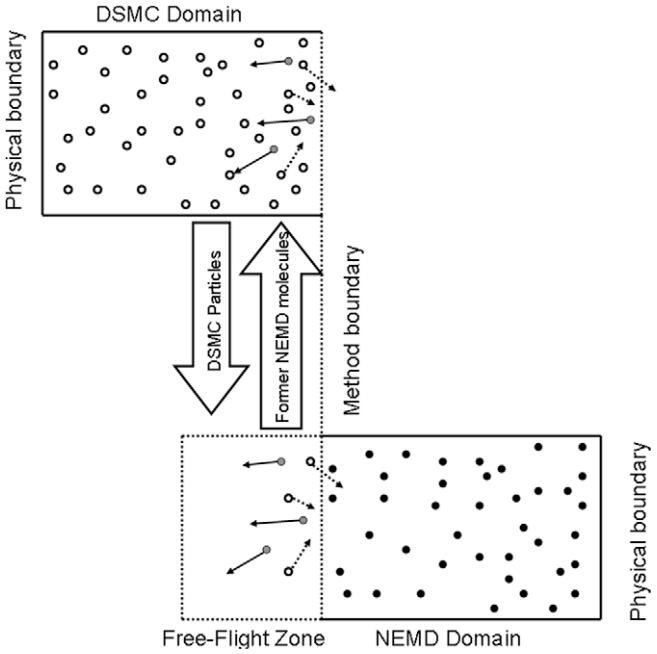

Fig. 5. Conceptual diagram for inter-method particle exchange at synchronization. ○ open circle dot: DSMC particles; • black dot: NEMD molecules ●; grey dot: former NEMD molecules; dashed arrow: DSMC velocity vector; solid arrow: NEMD velocity vector.

Further reduction in the DSMC time step to approach the NEMD time step reduces the DSMC computational efficiency. It should be noted that the number of particles is not conserved in the NEMD domain. Since particles leave the dilute gas NEMD domain, the small time period $20\Delta\tau_{MD}$ between coupling steps, based on Verlet list principles, in effect, assures that during such a small time period, particle interactions are not influenced by adding and removing molecules.

DSMC time steps considerably larger than $20\Delta\tau_{MD}$ still produced good results in some of our preliminary simulations. Therefore, if needed, we can expand the DSMC time steps in regions further from the method interface, where a larger time step will not affect the hybrid coupling. This is unnecessary for the systems studied in the present research because the physical scale is small for DSMC and most of the computational overhead is due to the NEMD solver. Obviously, for multiscale problems with a much larger upper scale, the present method could be embedded within a continuum/DSMC hybrid.

The simulation method is explicitly designed for nonequilibrium processes and does not correspond to any of the standard statistical mechanical equilibrium ensembles. As a matter of normal statistical averaging, we use an "experimental" ensemble based on averaging over repetitions of the calculation with different random number seeds and therefore a different set of initial velocities and positions.

4. Validation of the method

The newly developed DSMC/NEMD method, which has no buffer zone, raises the question of whether the method interface is continuous in a particle sense and physically realistic. To validate the method and its boundary treatment, we chose three benchmark problems, an equilibrium gas system between isothermal diffusive walls, a Fourier thermal system and an oscillatory Couette flow. In the NEMD solver, molecular motions are driven by intermolecular forces derived from Eq. (1) with the force cut-off distance, $r_c = 2.5\sigma$.

The stress tensor and the heat flux vector components are calculated as

$$P_{\alpha\beta J} = \frac{1}{V_J}\left(m\sum_{i=1}^{N_J} c'_{i,\alpha}c'_{i,\beta} + \sum_{i<j} F_{ij,\alpha}\mathbf{r}_{ij,\beta}\right) \tag{17}$$

$$q^{tot}_{\alpha J} = \frac{1}{V_j}\left[\sum_{i=1}^{N_J} c'_{i,\alpha}\left(\frac{1}{2}mc'^2_i + E^{pot}_i\right) + \frac{1}{2}\sum_{i,j}^{N_J}(\mathbf{F}_{ij}.\mathbf{c}'_i)r_{ij,\alpha}\right] \tag{18}$$

in which N_J is the number of molecules in the sampling cell J with volume, V; α and β indicate the x, y, or z direction; $c'_\alpha = c_\alpha - \overline{c_\alpha}$ is the thermal velocity in the α direction; and $F_{ij,\alpha}$ is the interaction force between molecule i and molecule j in the α direction; $r_{ij,\beta}$ is the interaction vector in the β direction; and E^{pot}_i is the potential energy of particle i. The first terms in Eqs. (17) and (18) represent the kinetic contributions, while the remaining terms, which are not included in the DSMC

solver, represent the interaction contributions and, for the heat flux, potential energy flux. In our simulation, argon gas is chosen with the initially uniform density, $n_0 = 0.001\sigma^{-3}$, and temperature, $T_0 = 1.0\frac{\varepsilon}{k_B}$. To achieve accurate results, we employed an average of 100 particles per cell in the DSMC solver. For steady solution, results were obtained by time averages over 2×10^6 NEMD steps, and unsteady solution samples contained ensemble averages of over 1.5×10^7 molecules in a computational cell.

4.1. Equilibrium gas system and Fourier thermal system

In the equilibrium gas system and Fourier thermal system simulations, two thermally accommodating diffusive walls sit at the top and bottom of a gas domain. The DSMC solver is assigned to the lower-half y domain, while the NEMD solver is assigned to the upper-half y domain. Periodic boundary conditions are applied in the x and z (lateral) directions and Kn, based on the wall spacing, is around 1.25. Without a temperature difference between the diffusive walls, the system reaches an equilibrium state. For our validation purposes, we consider the distributions of the wall-perpendicular and lateral components of the outward velocity fluxes from the two domains, which can be determined from the following Maxwell–Boltzmann equilibrium distributions:

$$\begin{aligned} f_\alpha &= \pm 2\zeta_\alpha \exp(-\zeta_\alpha^2) \quad \alpha = y \\ f_\alpha &= \frac{1}{\sqrt{\pi}} \exp(-\zeta_\alpha^2) \quad \alpha = x, z \end{aligned} \tag{19}$$

where $\zeta_\alpha = c_\alpha / \sqrt{2k_B T/m}$ is the normalized thermal velocity component in the α direction, and the where the positive sign in the distribution function in the $\alpha = y$ direction refers to DSMC efflux and the negative sign refers to NEMD efflux.

Fig. 6 shows the results of the simulation velocity histogram data collected from sampling efflux particles in each domain near the solver domain interface. These data are compared with the Maxwell–Boltzmann distributions of Eq. (19). The efflux particle distribution statistics are consistent with Maxwell–Boltzmann equilibrium theory and demonstrate excellent agreement in particle exchange flux statistics, comparing the efflux distributions for the NEMD domain with the efflux distributions for the DSMC domain.

To examine the accuracy of the method for simulation of a nonequilibrium system, a Fourier flow system was also simulated. The physical configuration was the same as the equilibrium system except the upper wall temperature was set to The upper wall temperature was set to $2T_0$, with the lower wall temperature, $T_0 = 273$ K.

Sampling-obtained temperature and density from the DSMC/NEMD hybrid simulation and from a pure DSMC simulation for this system are shown in Fig. 7. The figure demonstrates good agreement of hybrid results with pure DSMC results.

The sampled heat fluxes for the two cases are shown in Fig. 8. The DSMC heat flux is continuous with the NEMD kinetic heat flux, and lower than that of the total NEMD heat flux because of the absence of the interaction and potential energy contributions. The overall heat flux discrepancy from the pure DSMC solution of approximately 1% is acceptably small.

For a moderately nonequilibrium system such as this one, the particle speed distribution can be expressed in the form of the first order Sonine polynomial expansion of the Chapman–Enskog distribution [27],

$$f^{CE}(\boldsymbol{\zeta}) = f^0(\boldsymbol{\zeta})\Gamma(\boldsymbol{\zeta}) \tag{20}$$

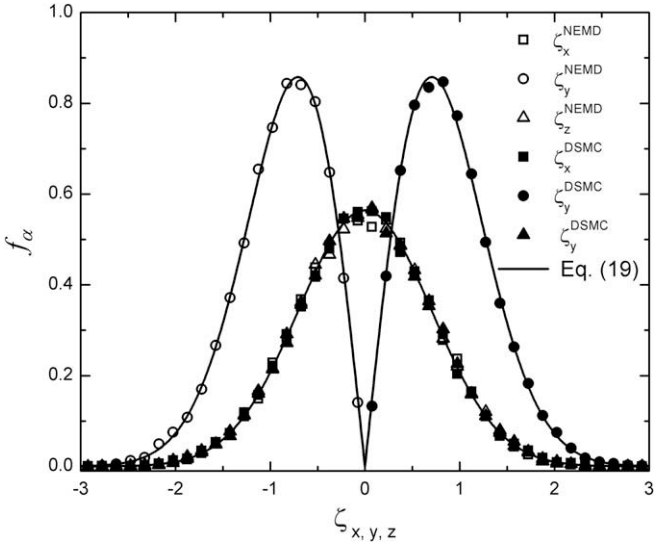

Fig. 6. Comparison of hybrid DSMC/NEMD, equilibrium, domain efflux statistics near inter-method interface with corresponding Maxwell–Boltzmann distributions [Eq. (19)]. Data point labels refer to the particle velocity data set from which the statistical histogram was constructed.

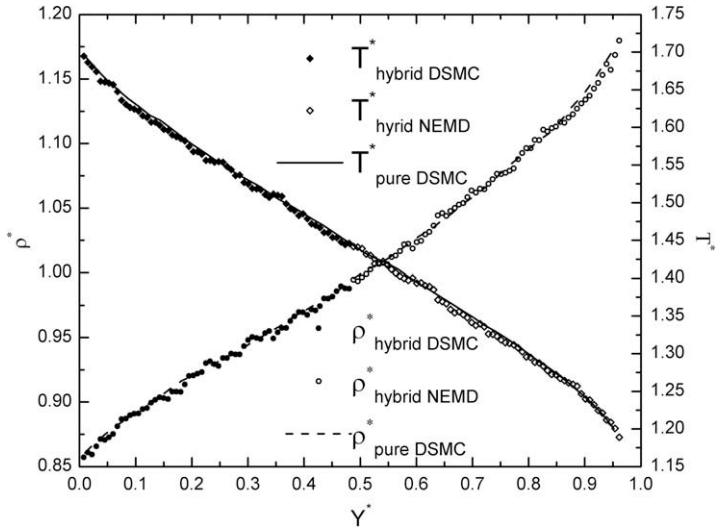

Fig. 7. Comparison of normalized Fourier temperature and density profiles. Density is normalized by initial density, ρ_0. Temperature is normalized by initial temperature, T_0. Wall distance coordinate is normalized by wall separation.

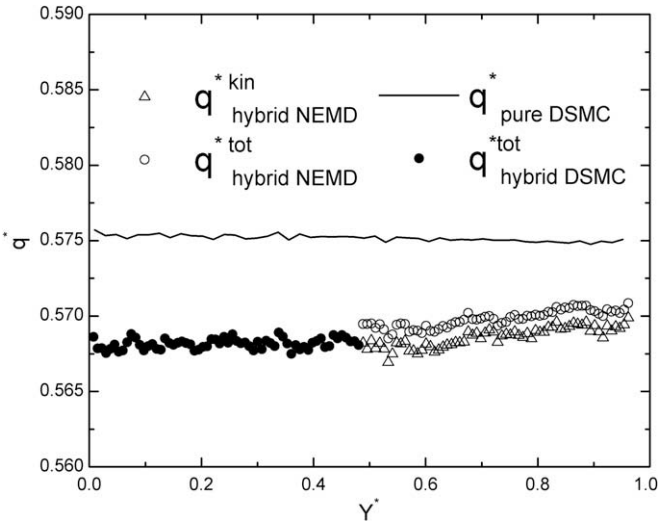

Fig. 8. Comparison of normalized Fourier heat flux profiles. Heat flux is normalized by $m^{-1/2}n_0(k_BT_0)^{3/2}$, where n_0 and T_0 are the initial number density and temperature, respectively. Wall distance coordinate is normalized by wall separation.

where

$$f^0(\zeta) = \prod_\alpha \frac{1}{\sqrt{\pi}} \exp(-\zeta_\alpha^2), \tag{21}$$

and

$$\Gamma(\zeta) = 1 + \left(\sum_\alpha q_\alpha^* \zeta_\alpha\right)\left(\frac{2}{5}\zeta^2 + 1\right) - \sum_{\alpha\neq\beta} \tau_{\alpha\beta}^* \zeta_\alpha \zeta_\beta - \tau_{xx}^*(\zeta_x^2 - \zeta_z^2) - \tau_{yy}^*(\zeta_y^2 - \zeta_z^2)$$
$$(\alpha, \beta = x, y, z) \tag{22}$$

In Eq. (22) $q_\alpha^* = \frac{1}{p}\sqrt{\frac{2m}{k_BT}} q_\alpha$ and $\tau_{\alpha\beta}^* = \frac{\tau_{\alpha\beta}}{p}$ are the normalized heat flux and viscous stress.

As in the validation of the hybrid method for the equilibrium case, we consider the distribution functions for the wall-perpendicular velocity efflux components and the lateral velocity efflux components from the two domains. These can be obtained as,

$$f_\alpha^{CE} = A_\alpha \int_{-\infty}^{+\infty} d\zeta_x \int_{-\infty}^{+\infty} d\zeta_z f^{CE}(\zeta)\zeta_\alpha \quad (\alpha = y)$$
$$f_\alpha^{CE} = A_\alpha \int_{-\infty}^{+\infty} d\zeta_\beta \int_{0/-\infty}^{+\infty/0} d\zeta_y f^{CE}(\zeta)\zeta_y \quad (\alpha,\beta) = (x,z) \quad \text{or } (z,x) \tag{23}$$

where ζ_y is evaluated from $-\infty$ to 0 for efflux from the NEMD domain toward the DSMC domain and from 0 to $+\infty$ for DSMC domain efflux toward the NEMD domain. Based on the fact that macroscopic gradients exist only in the y direction, A_α, the normalization parameter, is $A_\alpha = \frac{\pm 2\sqrt{\pi}}{(1-0.5\tau_{yy}^*)}$, where the positive sign refers to DSMC efflux and the negative sign refers to NEMD efflux.

In Figs. 9 and 10, histogram data obtained from the efflux particle velocities at locations near the DSMC/NEMD interface in each of the hybrid solver domains are compared with the corresponding Chapman–Enskog distributions computed from Eq. (23). The heat flux and stress components determined from the simulations are used to rescale Eq. (23) so that the distributions can be applied more confidently to the Knudsen number of the present case, which is slightly greater than 1. Given that the heat flux and shear stress components were not also obtained from theory, the theoretical and simulated results are not completely independent. Nevertheless, the excellent matching of the simulation data with the Chapman–Enskog distribution across the spectrum of particle speeds in these comparisons clearly illustrates that our DSMC/NEMD hybrid method captures the nonequilibrium statistical kinetic behavior of particles. This agreement extends to the nonequilibrium particle flux transferring from one solver to the other and it demonstrates that the artifice of a buffer zone is unnecessary.

4.2. Oscillatory Couette flow

The Fourier thermal flow results show that our DSMC/NEMD hybrid method produces good agreement with pure DSMC simulations for a steady nonequilibrium problem. To study the ability of the method to accurately simulate unsteady flow systems, we considered argon gas flow between two horizontal isothermal surfaces, the bottom of which is stationary and the top is oscillating in the x direction with velocity, $U_w = U_0 \sin(\omega t)$, where $U_0 = 0.63\sqrt{\varepsilon/m}$ is the magnitude of the velocity and ω is the oscillation frequency. Periodic boundary conditions are maintained in the other directions. The gas is initially at rest, with the same temperature, $T = 1.0\frac{\varepsilon}{k_B}$, as that at which the upper and lower wall will be maintained. The Stokes number, $\sqrt{\frac{mn_0\omega H^2}{\mu}}$, which represents the balance between the unsteady and viscous effects, equals 1.0 and and Kn = 0.81 in this simulation.

We assigned an MD solver to each of the upper and lower domains of the gas flow with a DSMC domain in the middle, so that each solver was responsible for a third of the region between the surfaces. Figs. 11 and 12 show the resulting hybrid velocity and shear stress profiles at four different time points ($t = 0.25t_0, t = 0.5t_0, t = 0.75t_0, t = t_0$, where t_0 is the period of the oscillation wall velocity) compared with a pure DSMC solution. The results in Figs. 11 and 12 demonstrate that our DSMC/NEMD hybrid method captures the time response of the system quite well, without any unphysical manipulations or artifices.

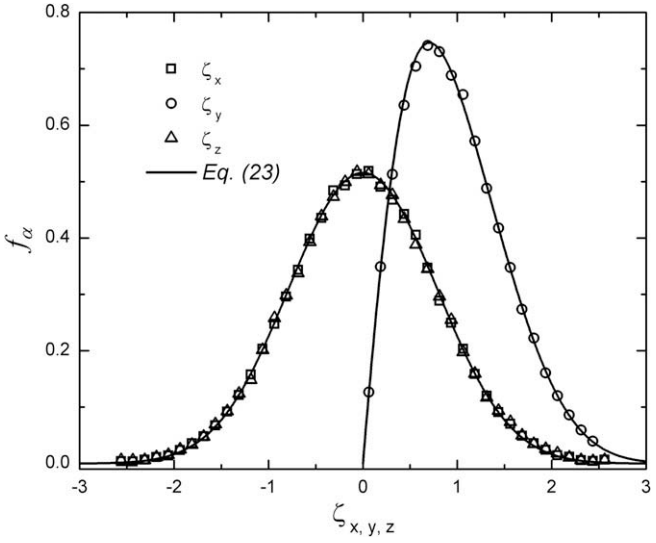

Fig. 9. Comparison of Fourier flow hybrid DSMC/NEMD, nonequilibrium DSMC efflux statistics near inter-method interface with corresponding Chapman–Enskog distributions [Eq. (23)]. Data point labels refer to the particle velocity data set from which the statistical histogram was constructed.

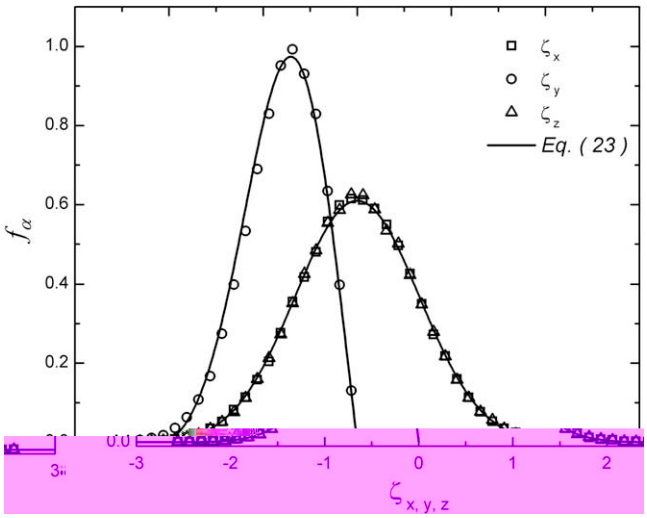

Fig. 10. Comparison of Fourier flow hybrid DSMC/NEMD, nonequilibrium NEMD efflux statistics near inter-method interface with corresponding Chapman–Enskog distributions [Eq. (23)]. Data point labels refer to the particle velocity data set from which the statistical histogram was constructed.

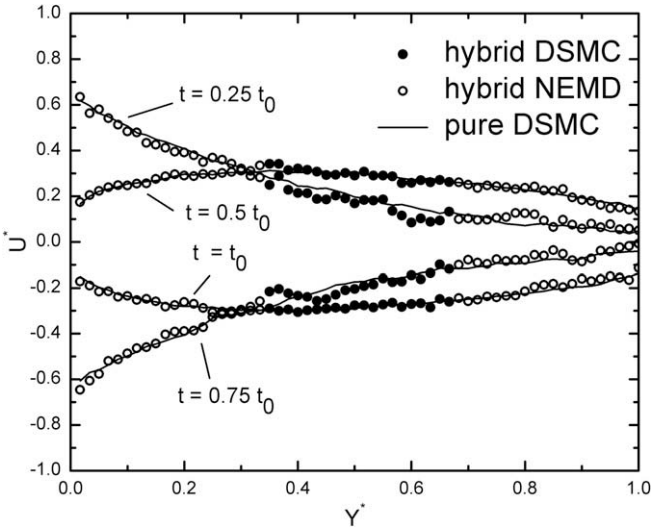

Fig. 11. Comparison of oscillating Couette flow normalized velocity profiles. Velocity is normalized by the magnitude of oscillatory wall velocity, U_0. Wall distance coordinate is normalized by wall separation.

The pure DSMC simulation of Figs. 11 and 12 is, again, performed with our DSMC formulation using MGSS. In testing the MGSS model, we also performed a DSMC simulation of the Couette system and the thermal system in the preceding section with Bird's VHS [1] collision model. The results, not shown here, were compared with a pure NEMD solution and demonstrated the improved accuracy of the MGSS model over VHS for shear stress in the Couette system and heat flux in the thermal system. This was expected, given the better fits for GSS and, hence, MGSS with the L-J potential and the better experimental agreement of GSS compared with VHS [24].

5. Assessment of computational performance

To assess the computational performance of the hybrid method, we compared the hybrid CPU times in the simulation of the equilibrium gas system for three different partitions of the region between the isothermal diffusive walls into NEMD and DSMC domains. Systems were simulated containing 8000, 16,000, and 32,000 gas molecules. For each size of the system, we chose three different values for the NEMD/DSMC solver partition ratio, r_{MD}: 25%, 50%, and 100% . To facilitate the comparison, the hybrid codes were executed by the serial processor.

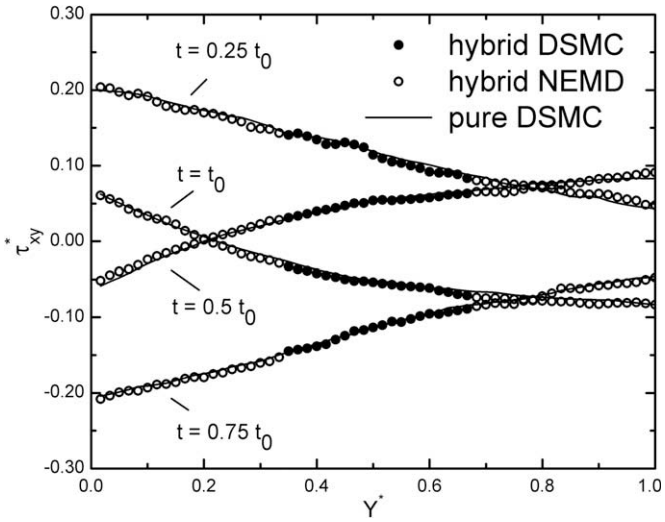

Fig. 12. Comparison of oscillating Couette flow normalized shear stress profiles. Shear stress is normalized by p_0, the initial pressure. Wall distance coordinate is normalized by wall separation.

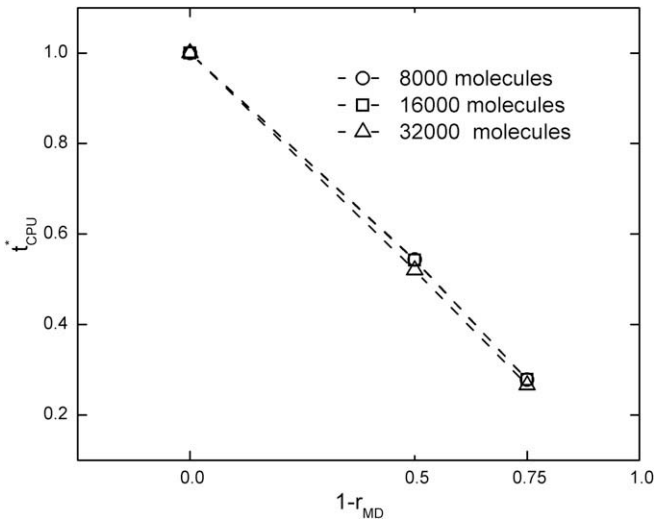

Fig. 13. Normalized CPU time dependence on solver partition fraction for different system sizes.

The results of the solver split and system size comparisons are shown in Fig. 13, where the x axis represents the DSMC partition fraction, $1 - r_{MD}$. The CPU time, normalized by the pure NEMD CPU time for each system size, t^*_{CPU}, was determined for 2×10^5 hybrid NEMD steps, which are equivalent to 10^4 hybrid DSMC steps. It is apparent that the CPU time is reduced substantially by reducing the NEMD solver partition and increasing the DSMC solver partition.

Our performance results compare favorably with the increase in computational efficiency due to hybridization reported by Nedea et al. [19]. In the present study, for 25% MD-75% DSMC, the CPU time is reduced by 80% and for 50% MD-50% DSMC, the CPU time is reduced by 50%. For the dilute gas case of [19], at 10% MD-90% MC, the CPU time is reduced by 82%, whereas for the partition studied in common with our investigation, 50% MD-50% MC, the CPU time is reduced by less than 1%. However, an indisputable determination of which algorithm is more efficient is not possible from the results presented due to differences in the densities of the systems studied and the degrees of parallelization.

The CPU time scales with the system size for both solvers in the present testing. The DSMC solver is at least ten times more efficient than the MD solver for particle statistics within the coupling procedure. However, even though an order of magnitude increase in performance is achieved at the particle level, the DSMC solver algorithm produces some non-physical noise due to its probabilistic nature, which may require more sampling than the NEMD statistics if accurate macroscopic properties in the DSMC domain are of interest. On the other hand, the "memory" scale of NEMD molecules is short and, as a consequence, DSMC noise will not penetrate very far into the NEMD domain so NEMD sampling to obtain macroscopic properties there should not be affected.

Although it was not attempted in the present investigation, a strategy to reduce the DSMC noise in the parallel implementation of the method, where DSMC is assigned to a separate processor, is to make use of the dead time in the DSMC processor after a DSMC time step, while the processor is waiting for the NEMD processor to catch up. Thus, better load balance would be achieved.

Table 1
Accommodation coefficient cases with DSMC comparisons.

	$T_0 = 1.0\frac{\varepsilon}{k_B}$		$T_0 = 2.0\frac{\varepsilon}{k_B}$	
	a_n	a_t	a_n	a_t
$m_s = 100m_g, \varepsilon_{sg} = 1.0$	0.15	0.15	0.085	0.14
$m_s = 25m_g, \varepsilon_{sg} = 1.0$	0.40	0.41	0.30	0.30
$m_s = 25m_g, \varepsilon_{sg} = 0.5$	0.19	0.19	0.17	0.19

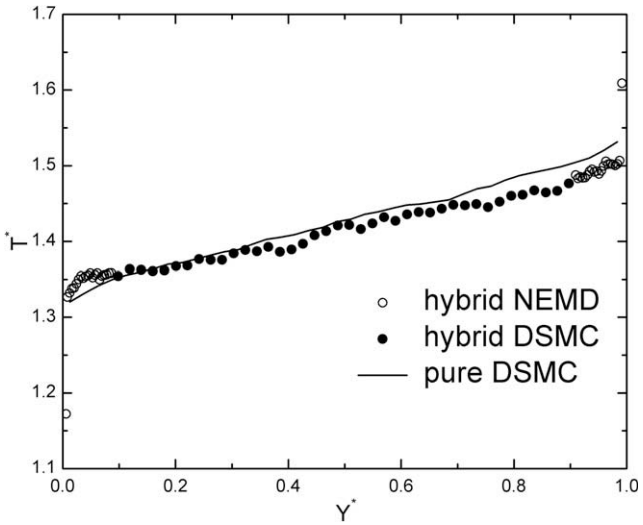

Fig. 14. Normalized temperature profiles for solid molecule wall case: $m_s = 100m_g, \varepsilon_{sg} = 1.0$. Temperature is normalized by initial temperature, T_0. Wall distance coordinate is normalized by mean wall separation.

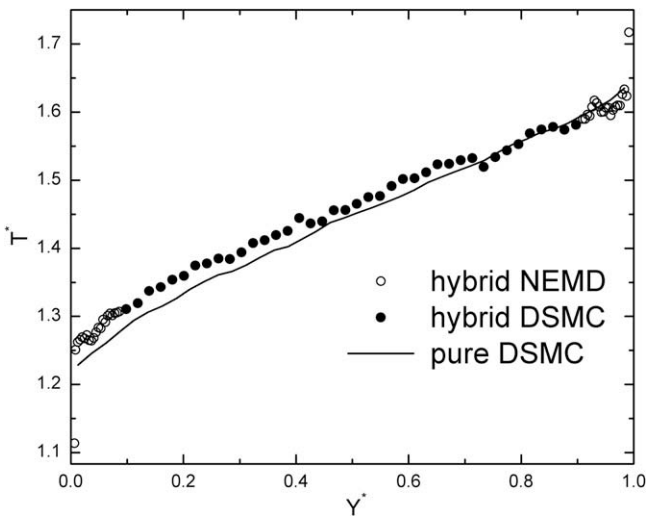

Fig. 15. Normalized temperature profiles for solid molecule wall case: $m_s = 25m_g, \varepsilon_{sg} = 1.0$. Temperature is normalized by initial temperature, T_0. Wall distance coordinate is normalized by mean wall separation.

One way of doing this is to employ a kind of micro ensemble averaging. This would involve replaying the DSMC collision calculation with different random number seeds to produce independent additional DSMC realizations of post-collision velocities and resulting particle displacements, i.e., phase space coordinates within the DSMC time step. The cell-sampled particle statistics for these micro ensembles would then be averaged to produce a cell micro sample used as the basis for the overall time or ensemble averaging process in place of a single sample for a cell at a time step. In addition, the phase space coordinates of the multiple DSMC realizations within a time step could be suitably sampled to statistically improve the set of particle locations and velocities used as input to the next DSMC collision time step.

6. Application of method to investigate thermal accommodation at a surface

One of the advantages for using the NEMD method at a surface is its capability of studying the physics of interface phenomena. One use of this capability is the determination of the thermal accommodation coefficient often used as an approximate boundary condition for molecular interaction surface physics in kinetic theory-based computations such as DSMC.

A thermal accommodation coefficient for total energy of molecules at the gas–solid surface, a_E can be defined as cf. [18]

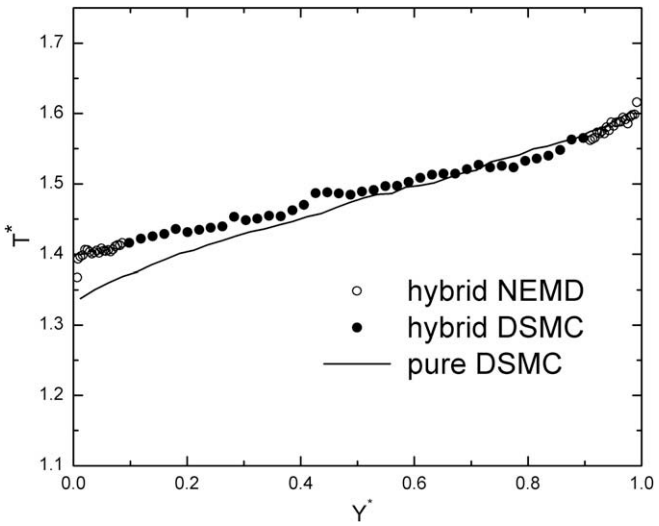

Fig. 16. Normalized temperature profiles for solid molecule wall case: $m_s = 25m_g, \varepsilon_{sg} = 0.5$. Temperature is normalized by initial temperature, T_0. Wall distance coordinate is normalized by mean wall separation.

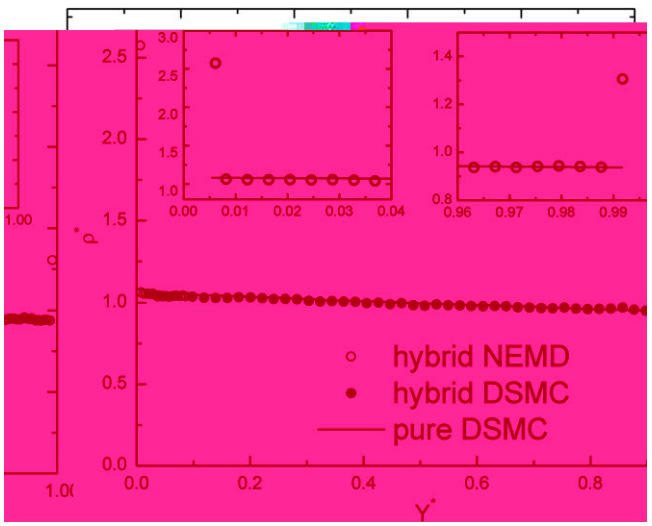

Fig. 17. Normalized density profiles for solid molecule wall case: $m_s = 100m_g, \varepsilon_{sg} = 1.0$. The left inset shows the density detail profiles near the cool wall. The right inset shows the density detail profiles near the hot wall. Density is normalized by initial density, ρ_0. Wall distance coordinate is normalized by mean wall separation.

$$a_E = \frac{\overline{E_i} - \overline{E_r}}{\overline{E_i} - \overline{E_w}} \tag{24}$$

where $\overline{E}$ is the total energy and subscripts i and r refer to the incident and reflected molecules, respectively. The subscript w indicates the molecules that would be outgoing in equilibrium with the wall under diffuse reflection. The accommodation coefficient of normal component, a_E^n, and tangential component, a_E^t, can be obtained from the energy in the normal and tangential directions to the solid surface, respectively.

Positing the Maxwell-type reflection condition that reflected particles are classified into two categories, equilibrium or specular reflection, Yamamoto et al. [18] address the accommodation coefficient of for energy in the following form, which allows the accommodation coefficient to be computed from NEMD simulation at the surface:

$$f^r = a_E f^w + (1 - a_E) f^{i-} \tag{25}$$

where f^w is the Maxwell–Boltzmann distribution described in Eq. (19) and f^{i-} is the distribution function of the incident molecules' specular reflections, which is determined from the statistics of simulated molecules, as is f^r

In the present gas–solid interaction simulation, we considered mesoscale wall phenomena in a micro-channel with two solid wall boundaries, formed by two FCC layer structures for each, separated by 10λ in the y direction. Periodic boundary

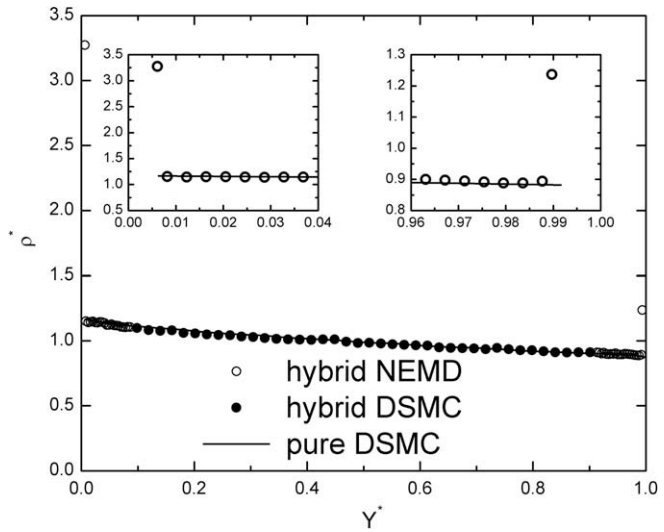

Fig. 18. Normalized density profiles for solid molecule wall case: $m_s = 25m_g, \varepsilon_{sg} = 1.0$. The left inset shows the density detail profiles near the cool wall. The right inset shows the density detail profiles near the hot wall. Density is normalized by initial density, ρ_0. Wall distance coordinate is normalized by mean wall separation.

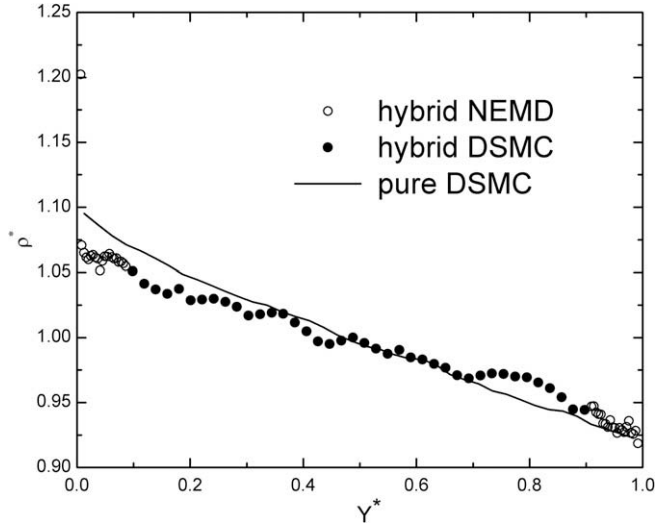

Fig. 19. Normalized density profiles for solid molecule wall case: $m_s = 25m_g, \varepsilon_{sg} = 0.5$. Density is normalized by initial density, ρ_0. Wall distance coordinate is normalized by mean wall separation.

conditions were applied in the x and z directions. The solid NEMD molecules employed in the hybrid simulations were tethered together and anchored within a FCC lattice by a fictitious spring force. Unlike the thermal diffusive wall simulations, the explicit solid wall temperatures for these hybrid simulations were controlled by a velocity rescaling method applied to the wall molecules.

The thermal accommodation coefficients were obtained from our hybrid simulations by calculating the incident (f^i) and reflected molecular distributions (f^r) at a distance r_c away from the mean solid surface. Applying Eq. (25), the thermal accommodation coefficient, assuming the Maxwell-like reflection condition, was readily obtained. In these simulations, the NEMD solvers were assigned to the regions comprising the solid walls and the gas just above them, while a DSMC solver was devoted to the remaining computational space in the middle. Each NEMD solver domain occupied 8.33% of the computational space and the DSMC domain was devoted to the remaining 83.33%. The temperature of the upper solid wall was twice the lower wall temperature, T_0. A steady state was reached after 10^7 NEMD steps. To reduce statistical fluctuations to an acceptable level, the macroscopic properties were obtained by averaging over 4×10^6 NEMD steps after steady state is reached, with around 10^8 MD samples per cell and 1.6×10^7 DSMC samples per cell. NEMD cells are defined merely for sampling purposes and were selected as the minimum size to yield good spatial resolution while encompassing an adequate number of particles to yield a meaningful sample.

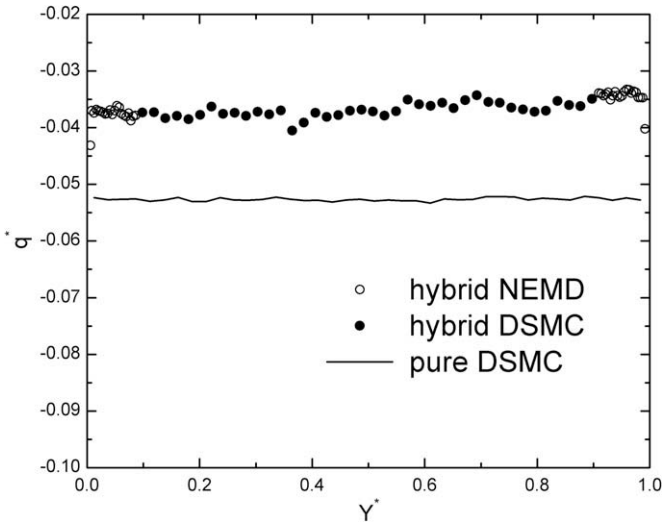

Fig. 20. Normalized heat flux profiles for solid molecule wall case: $m_s = 100m_g, \varepsilon_{sg} = 1.0$. Heat flux is normalized by $m^{-1/2}n_0(k_BT_0)^{3/2}$, where n_0 and T_0 are the initial number density and temperature, respectively. Wall distance coordinate is normalized by mean wall separation.

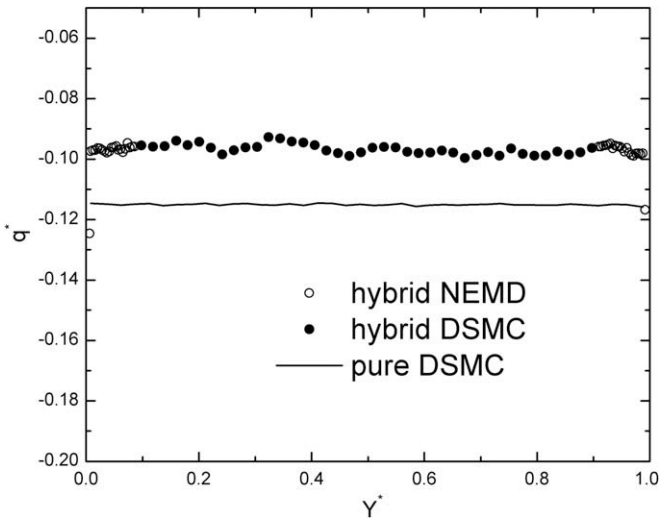

Fig. 21. Normalized heat flux profiles for solid molecule wall case: $m_s = 25m_g, \varepsilon_{sg} = 1.0$. Heat flux is normalized by $m^{-1/2}n_0(k_BT_0)^{3/2}$, where n_0 and T_0 are the initial number density and temperature, respectively. Wall distance coordinate is normalized by mean wall separation.

Accommodation coefficients from several simulations with different L-J gas–solid interaction parameters, ε_{sg}, and ratios of solid particle mass, m_s, to gas particle mass m_g are compared in Table 1.

Figs. 14–22 show the temperature, density, and heat flux results, respectively, from the hybrid simulations for the parameter sets of Table 1. They are compared with the results of pure DSMC simulations that used the accommodation coefficients obtained from the hybrid simulations and shown in Table 1. Three cases, large m_s with complete wetting ($m_s = 100m_g, \varepsilon_{sg} = 1.0$), small m_s with complete wetting ($m_s = 25m_g, \varepsilon_{sg} = 1.0$), and small m_s with non-wetting ($m_s = 25m_g, \varepsilon_{sg} = 0.5$) are compared. From the hybrid results, the density achieves a higher value near the wall for $\varepsilon_{sg} = 1.0$ than for $\varepsilon_{sg} = 0.5$. Because of weaker interaction taking place, the case of $m_s = 25m_g$, $\varepsilon_{sg} = 0.5$ has a larger temperature slip than the case of $m_s = 25m_g, \varepsilon_{sg} = 1.0$. On the other hand, the completely wetting wall of $m_s = 100m_g$ has a larger temperature slip than the completely wetting wall of $m_s = 25m_g$.

DSMC, with an accommodation coefficient determined from applying the Maxwell condition to the hybrid simulation, was able to reproduce the temperature profile away from the wall, including the apparent "slip" temperature with only a slight discrepancy as shown in Figs. 14–16. However, as shown in Figs. 20–22, it could not describe the temperature and density variations and wetting effect closer to the wall; neither could it describe the energy flux across the solid–gas interface with the result that its computed overall heat flux is erroneous.

In Figs. 23 and 24, the normal and tangential thermal accommodation coefficients of the upper wall are shown in relation to m_s and ε_{sg}, separately for the cases of Table 1 with some additional parameter sets added. The accommodation coefficients

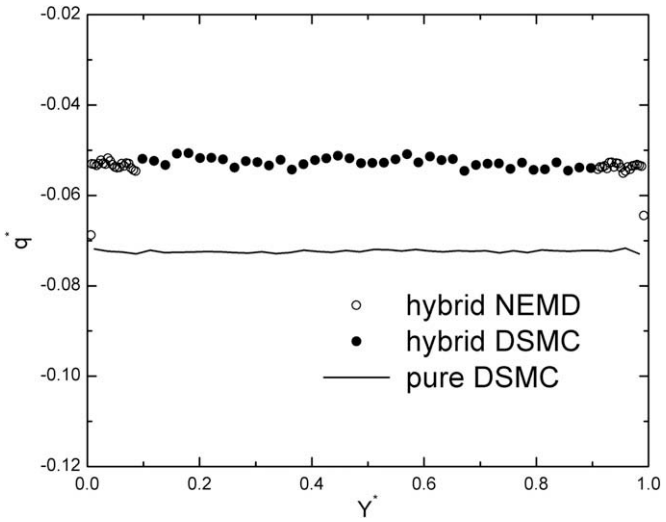

Fig. 22. Normalized heat flux profiles for solid molecule wall case: $m_s = 25m_g, \varepsilon_{sg} = 0.5$. Heat flux is normalized by $m^{-1/2}n_0(k_BT_0)^{3/2}$, where n_0 and T_0 are the initial number density and temperature, respectively. Wall distance coordinate is normalized by mean wall separation.

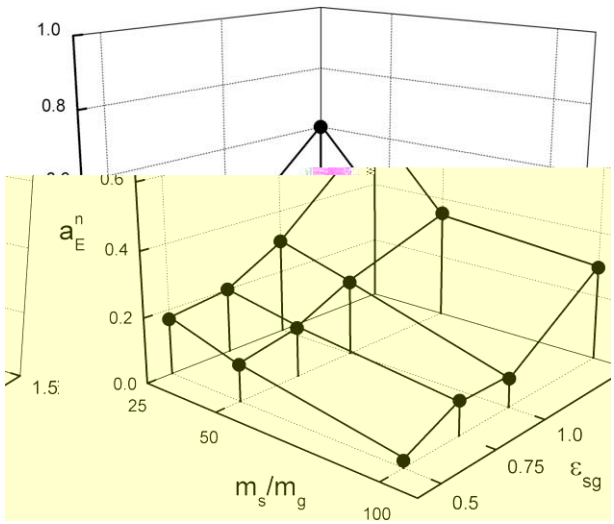

Fig. 23. Normal accommodation coefficient variation for simulated solid molecule wall cases.

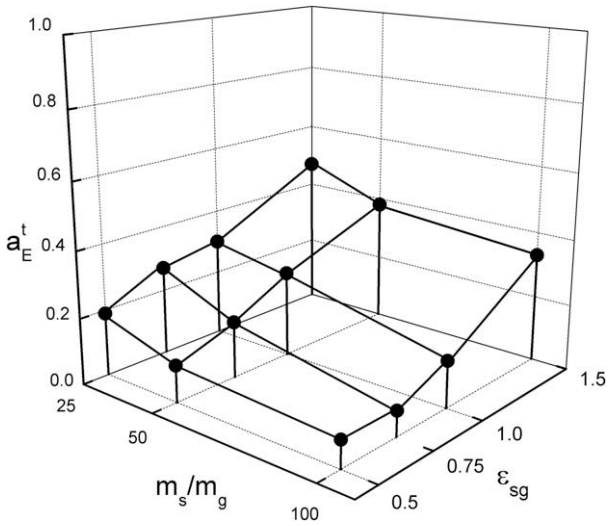

Fig. 24. Tangential accommodation coefficient variation for simulated solid molecule wall cases.

increase with an increase in the wetting effect. Molecules tend to spend more time near the solid molecules with a large ε_{sg} than a small ε_{sg}. Hence, more energy is transferred from solid phase to gas phase, reducing the temperature slip and thermal residence. Similarly, with small m_s, the relative surface energy accommodation of the wall also increases. Considering a single interaction between one gas molecule and one solid molecule, a smaller m_s achieves more energy transfer from the solid to the gas in the interaction. The small m_s wall molecules have larger vibrational amplitudes and frequencies than the large m_s wall molecules. Thus, the much smaller incident-gas molecules have more frequent and stronger energy exchanging interactions with the small wall molecules. These effects on molecular energy exchange account for all the variation of the accommodation coefficients with m_s and ε_{sg} shown in Figs. 23 and 24.

7. Conclusions

The atomistic hybrid DSMC/NEMD simulation method developed shows great promise as a versatile tool for investigating multiscale interfacial systems involving Knudsen layer gas flow over a surface with nanoscale surface interaction phenomena. It offers a distinct performance advantage over the use of NEMD alone for investigating such systems and does not depend on physically questionable artifices for its implementation. The generalized soft sphere DSMC collision model developed in conjunction with the hybrid method represents a significant advance in the selection of collision models available for use with DSMC.

The application of the hybrid method to study mesoscale molecular gas–solid interaction in a thermal driven Fourier system with different solid molecule masses, m_s, and gas–solid interaction parameters, ε_{sg}, illustrates the interesting results that can be obtained with the method. It was determined that solid to gas energy transfer increases with the wetting effect at the gas–solid interfaces. Furthermore, the smaller the solid mass, the more energy is transferred from solid to gas phase. The magnitude of both the normal and tangent accommodation coefficients follow the same trend as the energy transfer.

Applying the accommodation coefficients computed from the hybrid method in a pure DSMC simulation demonstrated an ability of the DSMC method to reproduce the same temperature slip near the wall as the hybrid. However, it was not able to capture the temperature and density variation closer to the gas–solid interface or the contribution to the heat flux from the surface energy transfer phenomena that were captured by the hybrid.

Acknowledgments

This work was supported by NSF Cooperative Agreement No. HRD-0206162, to the CREST Center for Mesoscopic Modeling and Simulation and NSF Award number 0934206 to the PREM, City College-Chicago MRSEC Partnership on the Dynamics of Heterogeneous and Particulate Materials.

References

[1] G.A. Bird, Molecular Gas Dynamics and the Direct Simulation of Gas Flows, Oxford, New York, 1994.
[2] E.S. Oran, C.K. Oh, B.Z. Cybyk, Direct simulation Monte Carlo: recent advances and applications, Ann. Rev. Fluid Mech. 30 (1998) 403–441.
[3] P.S. Prasanth, J.K. Kakkassery, Direct simulation Monte Carlo (DSMC): a numerical method for transition-regime flows – a review, J. Indian Inst. Sci. 86 (2006) 169–192.
[4] B.J. Alder, T.E. Wainwright, Studies in molecular dynamics. I. General method, J. Chem. Phys. 31 (1959) 459.

[5] D. Frenkel, B. Smit, Understanding Molecular Simulation, Academic, San Diego, 1996.
[6] D.C. Rapaport, The Art of Molecular Dynamics Simulation, second ed., Cambridge University Press, 2004.
[7] G. Abbate, C.R. Kleijn, B.J. Thijsse, Validation of a hybrid Navier–Stokes/DSMC method for multiscale transient and steady-state gas flows, Int. J. Mult. Comput. Eng. 6 (1) (2008) 1–12.
[8] Q. Sun, I.D. Boyd, G.V. Candler, A hybrid continuum/particle approach for modeling subsonic, rarefied gas flows, J. Comput. Phys. 194 (1) (2004) 256.
[9] Oz. Aktas, N.R. Aluru, A combined continuum/DSMC technique for multiscale analysis of microfluidic filters, J. Comput. Phys. 178 (2) (2002) 342.
[10] D.B. Hash, H.A. Hassan, Assessment of schemes for coupling Monte Carlo and Navier–Stokes solution methods, J. Thermophys. Heat Transfer 10 (2) (1996) 242.
[11] Y.-C. Wang, G.-W. He, A dynamic coupling model for hybrid atomistic-continuum computations, Chem. Eng. Sci. 62 (13) (2007) 3574.
[12] T. Werder, J.H. Walther, P. Koumoutsakos, Hybrid atomistic-continuum method for the simulation of dense fluid flows, J. Comput. Phys. 205 (1) (2006) 373.
[13] X.B. Nie, S.Y. Chen, W.N. E, M.O. Robbins, A continuum and molecular dynamics hybrid method for micro- and nano-fluid flow, J. Fluid Mech. 500 (2004) 55.
[14] R. Delgado-Buscalioni, P.V. Coveney, Continuum-particle hybrid coupling for mass, momentum, and energy transfers in unsteady fluid flow, Phys. Rev. E 67 (4) (2003) 0467041.
[15] E.G. Flekkoy, G. Wagner, G. Feder, Hybrid model for combined particle and continuum dynamics, Europhys. Lett. 52 (3) (2000) 271.
[16] H.S. Wijesinghe, R. Hornung, A.L. Garcia, N.G. Hadjiconstantinou, Three-dimensional hybrid continuum-atomistic simulations for multiscale hydrodynamics, J. Fluids Eng. 126 (2004) 768.
[17] M.I. Zeifman, B.J. Garrison, L.V. Zhigilei, Combined molecular dynamics – direct simulation Monte Carlo computational study of laser ablation plume evolution, J. Appl. Phys. 92 (4) (2002) 2181.
[18] K. Yamamoto, H. Takeuchi, T. Hyakutake, Characteristics of reflected gas molecules at a solid surface, Phys. Fluids 18 (2006) 046103.
[19] S.V. Nedea, A.J.H. Frijns, A.A. van Steenhoven, A.J. Markvoort, P.A.J. Hilbers, Hybrid method coupling molecular dynamics and Monte Carlo simulations to study the properties of gases in microchannels and nanochannels, Phys. Rev. E 72 (2005) 016705.
[20] S.V. Nedea , A.J. Markvoort, A.A. van Steenhoven, P.A.J. Hilbers, Heat transfer predictions for micro/nano-channels at atomistic level using combined molecular dynamics and Monte Carlo techniques, in: Proceedings of the Fifth International Conference on Nanochannels, Microchannels and Minichannels, ICNMM2007-30039, 2007.
[21] K. Koura, H. Matsumoto, Variable soft sphere molecular model for inverse-power-law or Leonard-Jones potential, Phys. Fluids A 3 (1991) 2459.
[22] H.A. Hassan, D. Hash, A generalized hard-sphere model for Monte Carlo simulation, Phys. Fluids A 5 (1993) 738.
[23] M.N. Macrossan, C.R. Lilley, Modified generalized hard sphere collision model for DSMC calculations, J. Thermphys. Heat Transfer 17 (2) (2003) 289.
[24] J. Fan, A generalized soft-sphere model for Monte Carlo simulation, Phys. Fluids 14 (12) (2002) 4399.
[25] J.O. Hirschfelder, C.F. Curtiss, R.B. Bird, Molecular Theory of Gases and Liquids, Wiley, New York, 1954.
[26] R. Delgado-Buscalioni, P.V. Coveney, An algorithm for particle insertion in dense fluid, J. Chem. Phys. 119 (2003) 978.
[27] S. Chapman, T.G. Cowling, The Mathematical Theory of Non-Uniform Gases, Cambridge Univ. Press, Cambridge, 1960.